Electronic Supplementary Material (ESI) for Chemical Communications.

Supporting Information of

[2.2]Paracyclophane-Bridged Platinum(II) Complexes for Silver(I) Recognition with Emission Enhancement

Yukui Tian,[a] Bin Chen,[a] Sixun Jiang,[b] Ming Yuan,[b] Jie Ren,[a] and Feng Wang*[b]*

[a] Institutes of Physical Science and Information Technology, Anhui University, Hefei, Anhui 230601, China. E-mail: tianyk@ahu.edu.cn

[b] Key Laboratory of Soft Matter Chemistry, Hefei National Laboratory for Physical Science at the Microscale, Department of Polymer Science and Engineering, University of Science and Technology of China, Hefei, Anhui 230026, China. E-mail: drfwang@ustc.edu.cn

Table of contents

1. Materials and Methods

Synthesis

Reagents and reactants: Copper(I) iodide (CuI) and trimethylamine were reagent grade and used as received. 4,15-diethynyl-[2.2]paracyclophane, 4-ethynyl[2.2]paracyclophane, [Pt($N^{t\text{-}Bu}$^$N^{t\text{-}Bu}$^$N^{t\text{-}Bu}$)Cl](BF_4) and [Pt(N^N^{phenyl}^N)Cl](BF_4) were synthesized according to the previously reported procedures.[S1-S4] Other reagents and solvents were employed as purchased.

Measurements

Instruments and characterization. ^{1}H NMR spectra was collected on a Varian Unity INOVA-400 spectrometer with TMS as the internal standard. Time-of-flight mass spectra (TOF-MS) were obtained on matrix-assisted laser desorption ionization-time of flight (autoflex speed TOF/TOF, Bruker). HPLC was performed on a Agilent system (1260 Infinity II) equipped with an DAD detector. UV/Vis spectra were recorded on a UV-1800 Shimadzu spectrometer. Transmission electron microscopy (TEM) experiments were performed on Tecnai G2 Spirit BioTWIN electron microscope (acceleration voltage: 120 kV). The hydrodynamic size distributions were characterized using dynamic light scattering (Malvern Zetasizer Nano ZS90).

DFT Theoretical calculations. DFT computations were performed by utilizing Gaussian 09 D.01 software package.[S6] During the optimization of ground state (S_0), Stuttgart effective core potential (SDD) was employed to describe Pt, Ag, and Cu atoms, while nonmetallic elements were calculated on PBE1PBE/6-31G(d) computational level. Time-dependent DFT (TD-DFT) was utilized to simulate the UV-Vis spectrum under the chloroform solvation conditions (PCM model). During the computation, Stuttgart effective core potential (SDD) was employed to describe Pt, Ag, and Cu atoms, while C, H, N, and O elements were calculated on the PBE1PBE/6-31G(d) level.

*Solvent-dependent mathematical model to fit the self-assembly curve of **4***. For the solvent-dependent UV–Vis measurements of **4**, a sigmoidal denaturation curve is obtained upon plotting α_{agg} *vs* the $CHCl_3$ volume fraction (*f*). The curve is fitted by an earlier reported equilibrium model adapted to solvent-dependent association using Matlab,[S5] which is described by **Eq. S1** and **Eq. S2**

$$\Delta G_f = \Delta G_0 + m \times f \qquad \textbf{(Eq. S1)}$$

$$K_e = \exp(-\Delta G_f / RT) \qquad \textbf{(Eq. S2)}$$

In this equation, ΔG_f is the Gibbs free energy of monomer association on the $CHCl_3$ volume fraction f, while ΔG_0 represents the Gibbs free energy gain upon monomer association in pure $CHCl_3$. The dependence of ΔG_f on f is described by the m-value. The assembly process is described as a sequence of monomer addition equilibria with equilibrium constant K_e as described in **Eq. S2**, where R is the gas constant, and T is the temperature.

*2. Spectroscopy of **1** and **4***

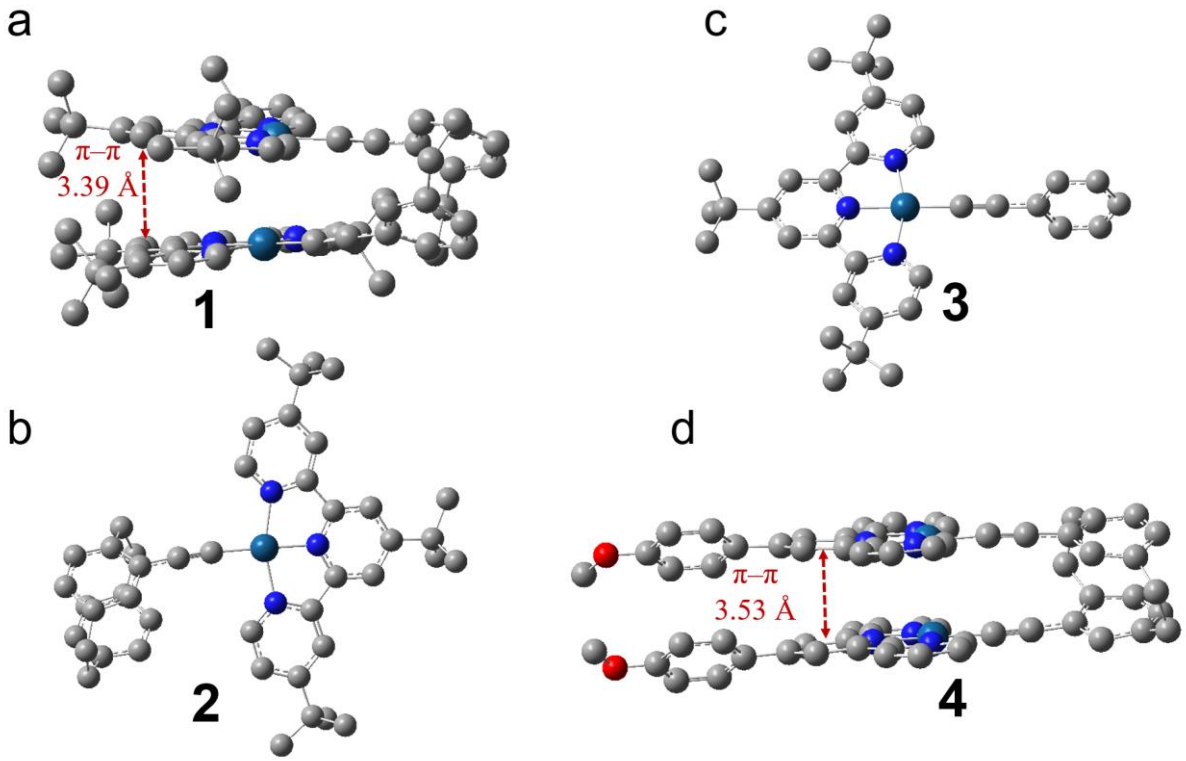

Figure S1. The optimized structure of compounds **1**–**4** on the basis of DFT computation (hydrogen atoms are omitted for clarity). The dodecyl chains units on **4** are replaced with methyl groups to reduce computational costs. For **1**, the π–π distance was determined to be 3.39 Å. The results denote the presence of intramolecular π–π stacking interaction between the two neighbouring Pt(II) pincers.

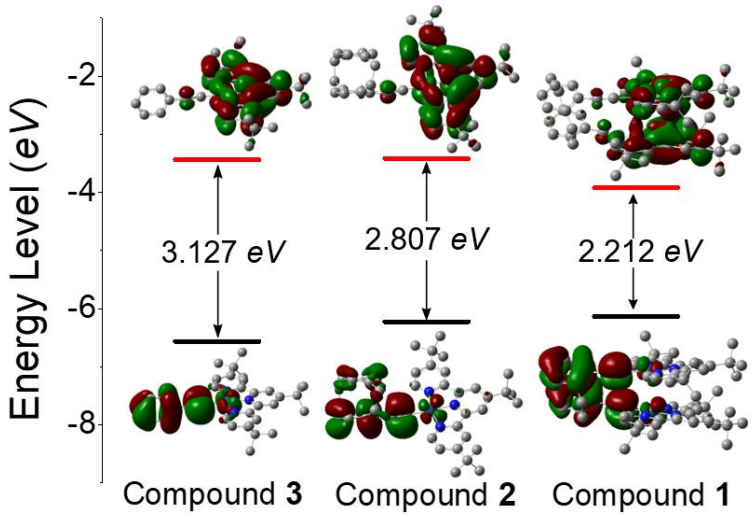

Figure S2. FMO energy levels and the corresponding electron densities (isovalue=0.02) of compounds **1**–**3**. The black lines and red lines mark the energy levels of HOMOs and LUMOs, respectively.

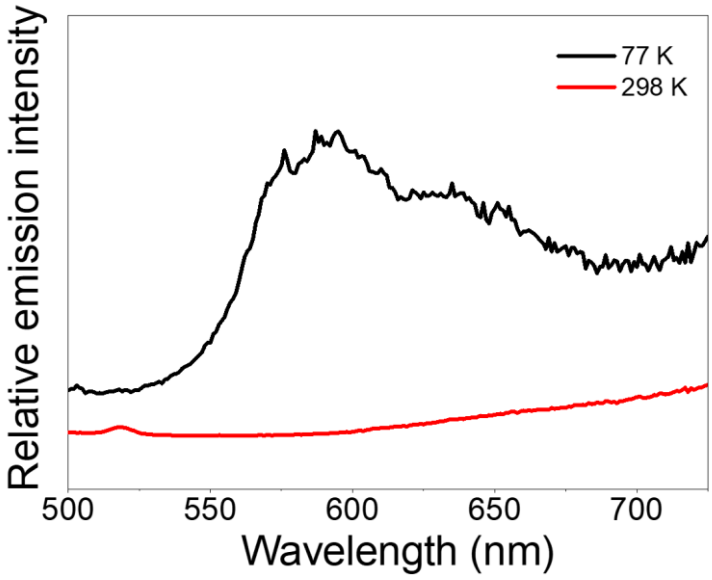

Figure S3. Emission spectra of **1** at 298 K and at 77 K (c = 1.00 $\times 10^{-4}$ M in 2-methyl tetrahydrofuran). As can be seen, in 2-methyltetrahydrofuran at 77 K (Fig. S3), no MMLCT emission band was detected for **1**. The MLCT/LLCT emission band of 1 centered at 580 nm is rather weak, albeit a little higher for the intensity than that at 298 K. Hence, the state-ment is changed in the manuscript to exclude the possibility of "Pt(II)---Pt(II) interactions" in **1**.

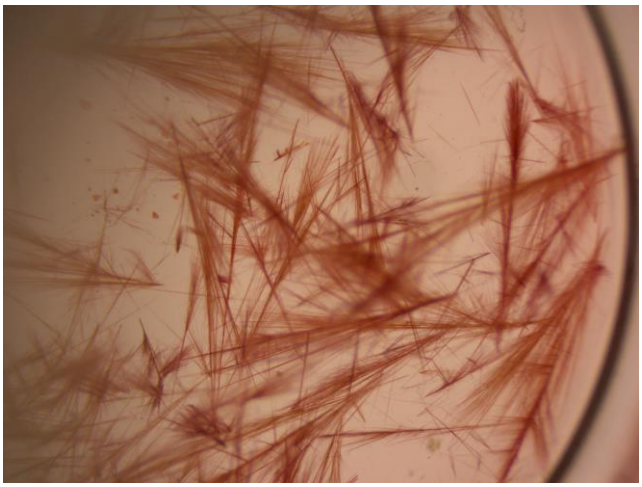

Figure S4. Crystal photos of compound **1**. Needle-like single crystals were obtained for **1** upon vapour diffusion of ethyl ether into the chloroform solution. Unfortunately, we failed to get the X-ray structures since these crystals were unstable under the desolvation conditions.

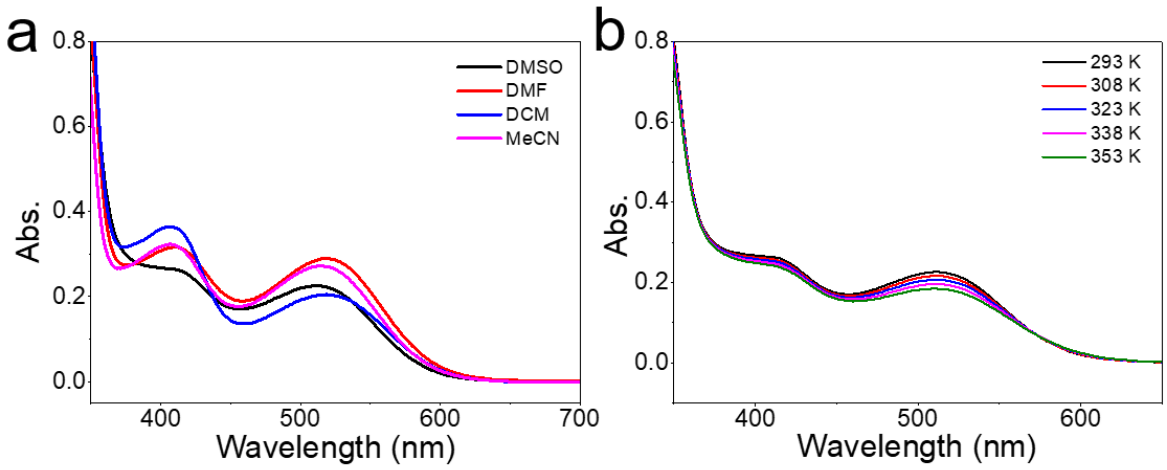

Figure S5. UV–Vis absorption spectral changes of **1** (c = 5.00 × 10^{-5} M) in different solvents (a), and in DMSO at different temperatures (b). Under these conditions, low-energy absorption bands exist between 550 and 600 nm. Accordingly, it demonstrates that the intramolecular π–π interaction in **1** are quite robust.

*3. Self-assembly of **4***

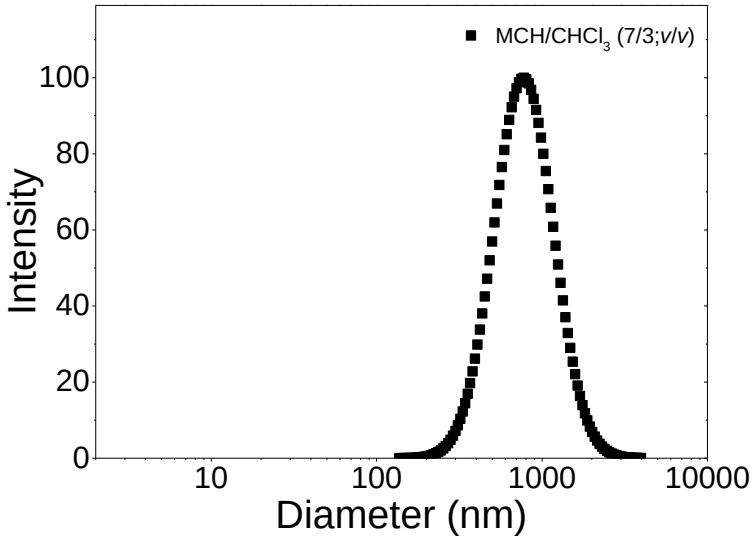

Figure S6. DLS measurements for **4** in MCH/$CHCl_3$ (7 : 3, *v*/*v*, $c = 5.00 \times 10^{-5}$ M).

*4. Ag^+ complexation behaviors of **1** - **4***

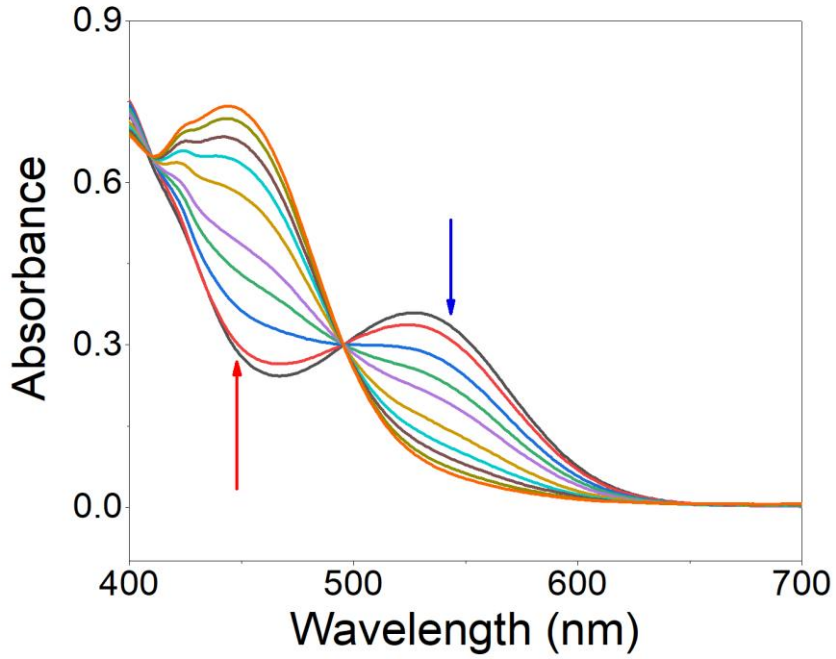

Figure S7. UV–Vis spectral changes of **1** upon gradual addition of Ag^+ ($CHCl_3/CH_3CN$ = 2 : 1, *v*/*v*; *c* = 7.00 × 10^{-5} M). Upon gradual addition of Ag^+ to the solution of **1**, a new absorbance band emerged at 463 nm, accompanied by the presence of an isosbestic point at 501 nm. The results indicate the formation of complex **1**⊃Ag^+.

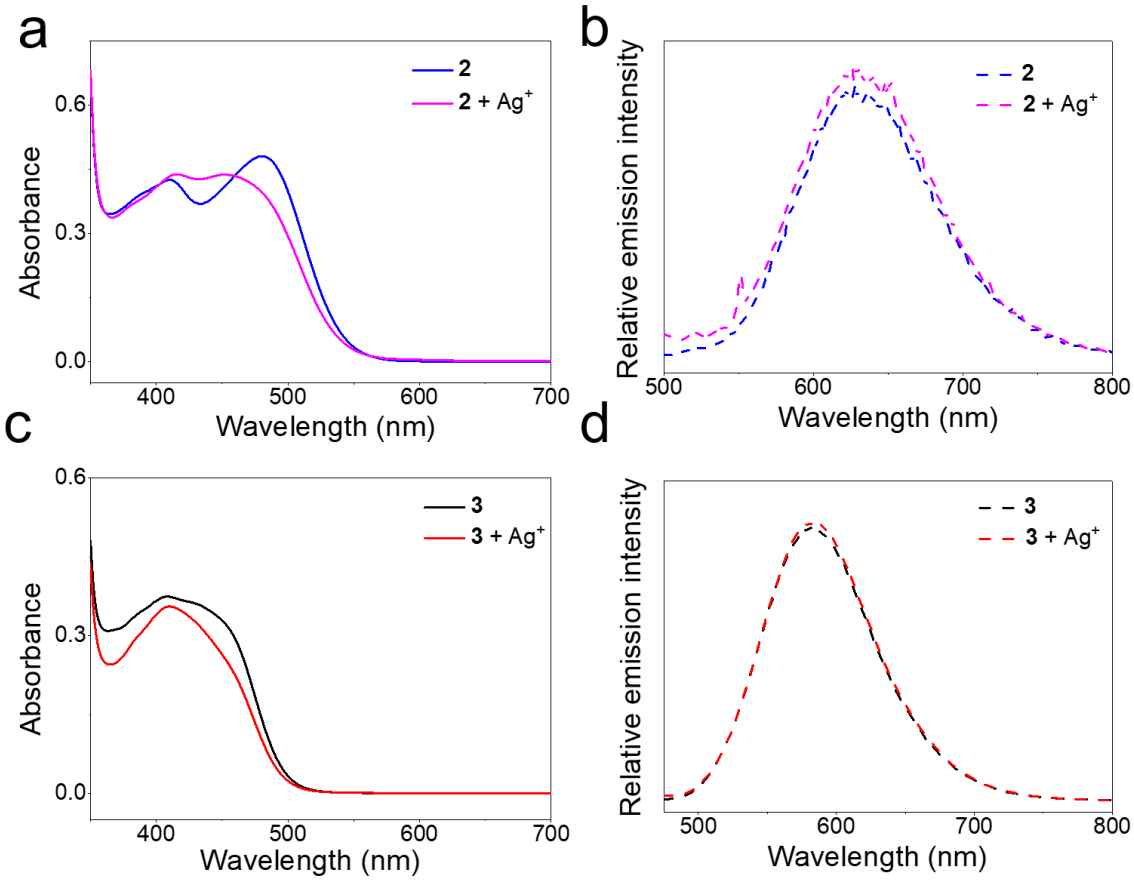

Figure S8. a) Absorption and b) emission spectra of **2** [c = 1.00 × 10^{-4} M in $CHCl_3$/CH_3CN (2 : 1, v/v)] upon the successive addition of $AgBF_4$. c) Absorption and d) emission spectra of **3** [c = 1.00 × 10^{-4} M in $CHCl_3$/CH_3CN (2 : 1, v/v)] upon the successive addition of $AgBF_4$. As shown in Fig. S8, for both **2** and **3** in $CHCl_3$/CH_3CN (2 : 1, v/v), the MLCT/LLCT absorption signals changed for their intensities upon addition of Ag^+, suggesting non-covalent complexation between compounds **2** (or **3**) and Ag^+. However, no emission signal changes occur for the resulting complexes (Fig. S8). It is evident that the adjacent acetylide units in **1** provide an inner cavity for Ag^+ recognition, which is absent in the cases of **2** and **3**. Accordingly, **1** is more prone to undergo adaptive conformational change than those of **2** and **3**, which are crucial for the emission "turn-on" behaviors upon recognizing Ag^+.

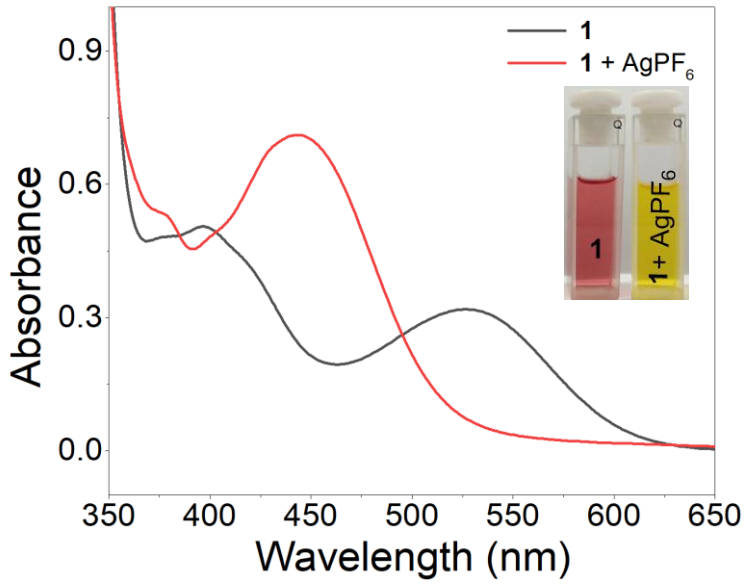

Figure S9. UV–Vis spectra of **1** [c = 6.00 × 10^{-5} M in $CH_3CN/CHCl_3$ (1 : 2, *v*/*v*)] upon addition of $AgPF_6$. Inset: photos of **1** with the presence of $AgPF_6$ under day light.

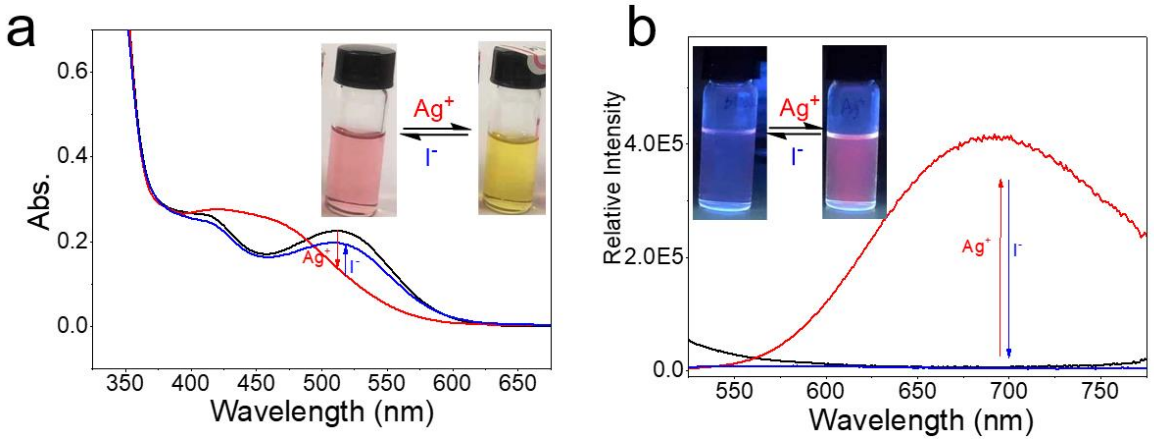

Figure S10. a) Absorption and b) emission spectra of **1** [5.00 × 10^{-5} M; $CH_3CN/CHCl_3$ (1 : 2, *v*/*v*)] upon the successive addition of $AgBF_4$ and Bu_4NI.

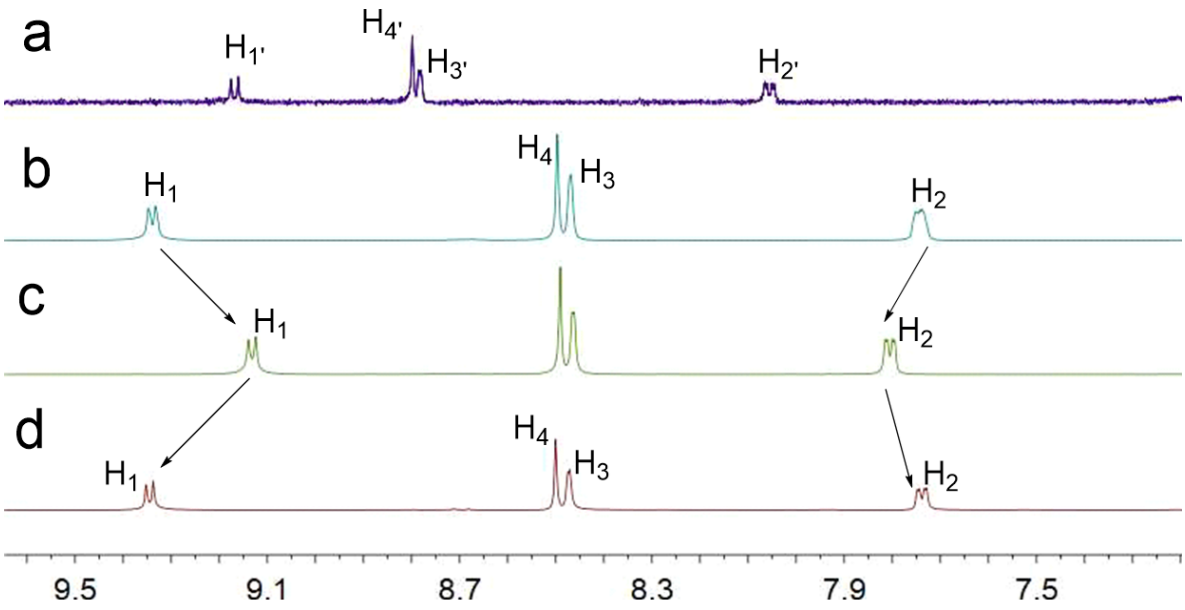

Figure S11. Partial ^{1}H NMR spectra (400 MHz, d_6-DMSO 298 K) of a) **2** (c = 2.00 × 10^{-3} M); b) **1** (c = 2.00 × 10^{-3} M); c) **1** upon addition of $AgBF_4$; d) **1** upon the successive addition of $AgBF_4$ and Bu_4NI.

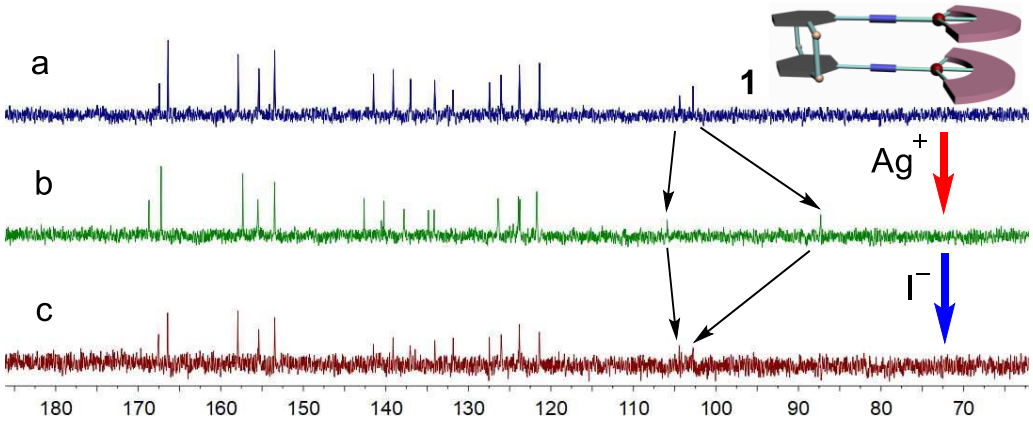

Figure S12. Partial ^{13}C NMR spectra (100 MHz, d_6-DMSO 298 K) of a) **1** (c = 8.00 × 10^{-3} M); b) **1** upon addition of $AgBF_4$; c) **1** upon the successive addition of $AgBF_4$ and Bu_4NI. In the ^{13}C NMR spectra, the acetylene resonances shifted dramatically from 103 and 104 ppm to 87.3 and 106 ppm, suggesting the formation of complex **1**⊃Ag^+. Meanwhile, I^- served as the competitive ligand to trigger the transformation from complex **1**⊃Ag^+ to **1**.

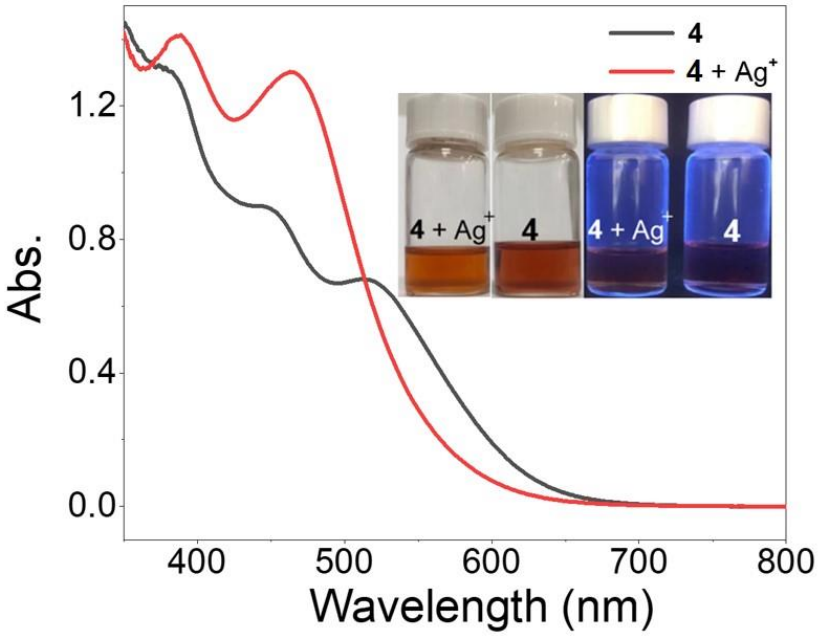

Figure S13. UV–Vis spectra of **4** [c = 4.00 × 10^{-5} M in $CH_3CN/CHCl_3$ (1 : 2, *v*/*v*)] upon addition of Ag^+. Inset: Photos of **4** with the presence of Ag^+ under day light (*Left*) and a 365 nm UV light (*Right*).

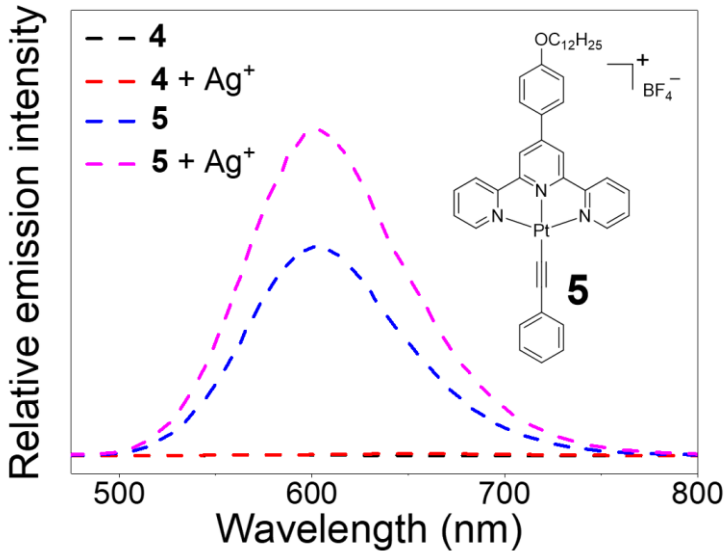

Figure S14. Emission spectra of **4** and **5** [the concentration of Pt(II) terpyridine units were kept at 1.00 × 10^{-4} M for both compounds, $CHCl_3/CH_3CN$ (2 : 1, *v*/*v*)] upon the successive addition of $AgBF_4$. As shown in Fig. S13, the emission intensity enhanced upon adding Ag+ into the CHCl3/CH3CN (2 : 1, v/v) solution of 5. The results exclude the impact of long alkoxyl chains to quench the emission signal.

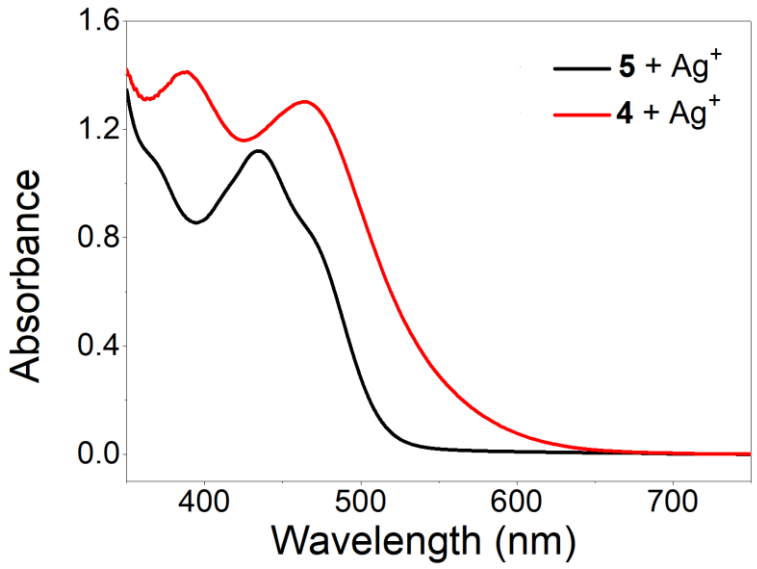

Figure S15. Absorption spectra of **4**⊃Ag^+ and **5**⊃Ag^+ in $CHCl_3/CH_3CN$ (2 : 1, *v*/*v*) [Pt(II) terpyridine pincers were kept at 8.00 × 10^{-5} M for both compounds]. The stronger intramolecular π–π stacking interaction in **4** than that of **1** attenuates Ag^+ binding affinity, leading to the different emission behaviors between **1** and **4** toward Ag^+. The conclusion can be manifested by the absorption signal changes between **4**⊃Ag^+ and **5**⊃Ag^+. As shown in Fig. S14, **4**⊃Ag^+ displays a low energy absorption band than that of **5**⊃Ag^+, supporting the existence of intramolecular π–π stacking interactions.

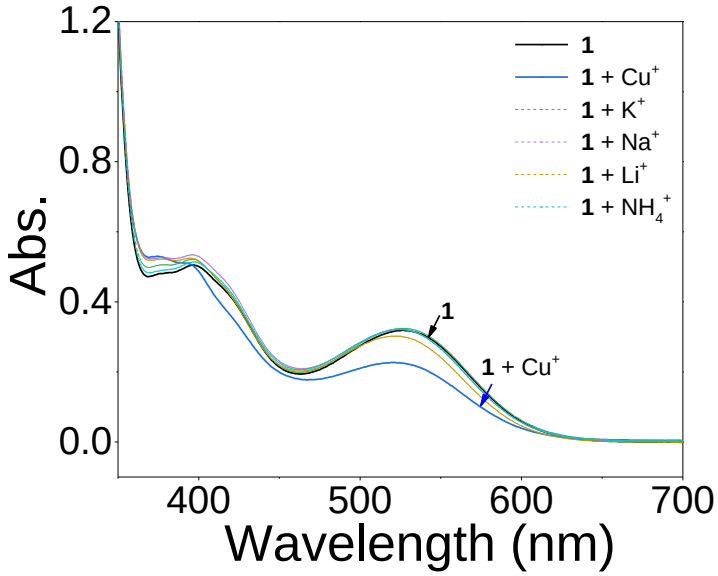

Figure S16. UV–Vis spectra of **1** [1.00 × 10^{-4} M; $CH_3CN/CHCl_3$ (1 : 2, *v*/*v*)] upon addition of various metal ions. As can be seen, the alkali metal ions and ammonium salt could not complex with compound **1**. Besides, although **1** is capable of sandwiching of Cu^+ between the neighboring η^2 acetylene ligands,[15] the color and emission signals hardly changed as well.

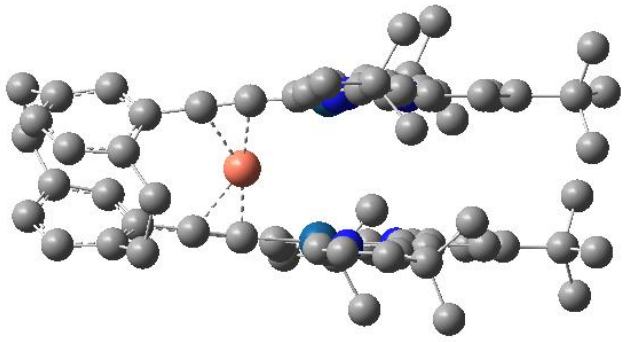

Figure S17. Optimized structures of complex **1**⊃Cu^{+} based on DFT calculation. The Pt(II)($N^{t\text{-}Bu}$^$N^{t\text{-}Bu}$^$N^{t\text{-}Bu}$) units are co-facial with each other in complex **1**⊃Cu^{+}, with the π−π distance of 3.81 Å.

*5. Synthetic routes to **1** and **4***

*5.1 Synthesis of compound **1***:

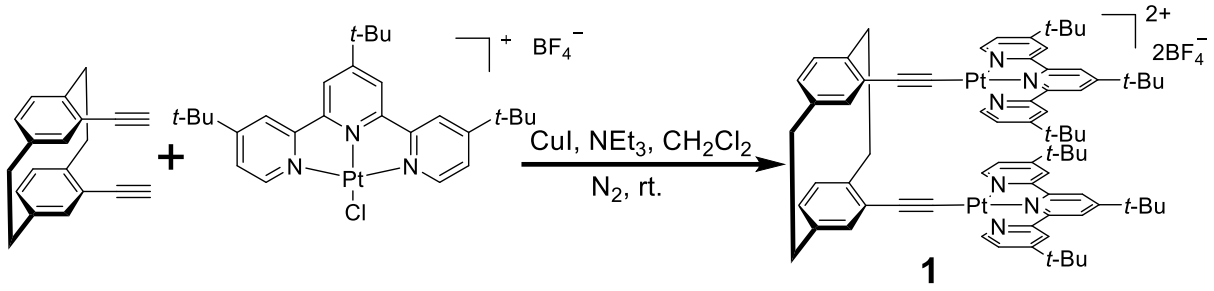

4,15-Diethynyl-[2.2]paracyclophane (50.0 mg, 0.19 mmol), [Pt($N^{t\text{-}Bu}$^$N^{t\text{-}Bu}$^$N^{t\text{-}Bu}$)Cl](BF_4) (0.28 g, 0.39 mmol), CuI (10.0 mg, 0.05 mmol), and NEt_3 (1 mL) in CH_2Cl_2 (10 mL) were stirred at room temperature for 24 hours. The mixture was evaporated under reduced pressure, and the residue was purified by flash column chromatography (Al_2O_3, CH_3OH/CH_2Cl_2, 1 : 100 *v*/*v* as the eluent) to afford **1** as a red solid (0.21 g, 68%). ^{1}H NMR (400 MHz, d_6-DMSO, 298 K, Figure S18) δ (ppm): 9.35 (d, J = 5.8 Hz, 2H), 8.50 (s, 4H), 8.47 (s, 4H), 7.75 (dd, J = 4.1, 1.6 Hz, 4H), 6.82 (s, 2H), 6.65 (d, J = 7.7 Hz, 2H), 6.49 (dd, J = 7.7, 1.3 Hz, 2H), 4.18 (d, J = 8.0 Hz, 2H), 3.19 (d, J = 8.1 Hz, 2H), 3.08 (s, 4H), 1.52 (s, 18H), 1.28 (s, 36H). ^{13}C NMR (100 MHz, d_6-DMSO, Figure S19) δ: 167.4, 166.4, 157.9, 155.4, 153.5, 141.5, 139.1, 136.9, 134.0, 131.9, 127.4, 126.0, 123.8, 121.4, 104.4, 102.7, 37.8, 36.6, 35.1, 34.4, 30.8, 30.2. MALDI−TOF−MS *m*/*z*: $[M–2BF_4]^{2+}$ calcd for $C_{74}H_{84}N_6Pt_2$, 723.3026; found, 723.1641 (Figure S21).

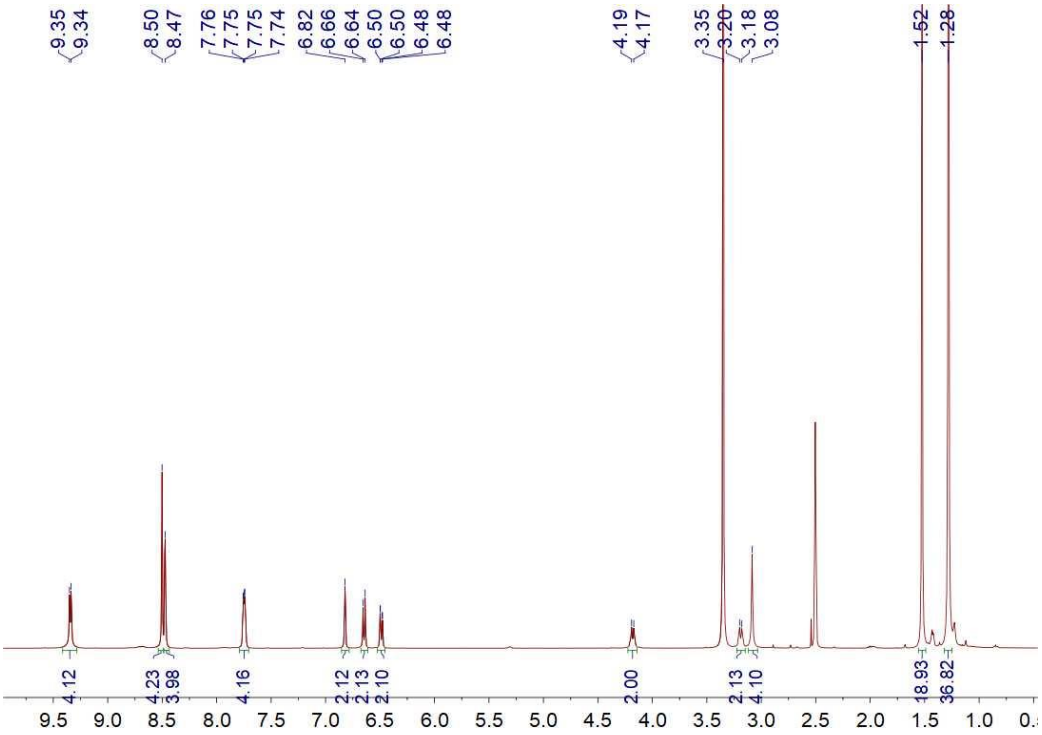

Figure S18. ^{1}H NMR spectrum (400 MHz, d_6-DMSO, 298K) of **1**.

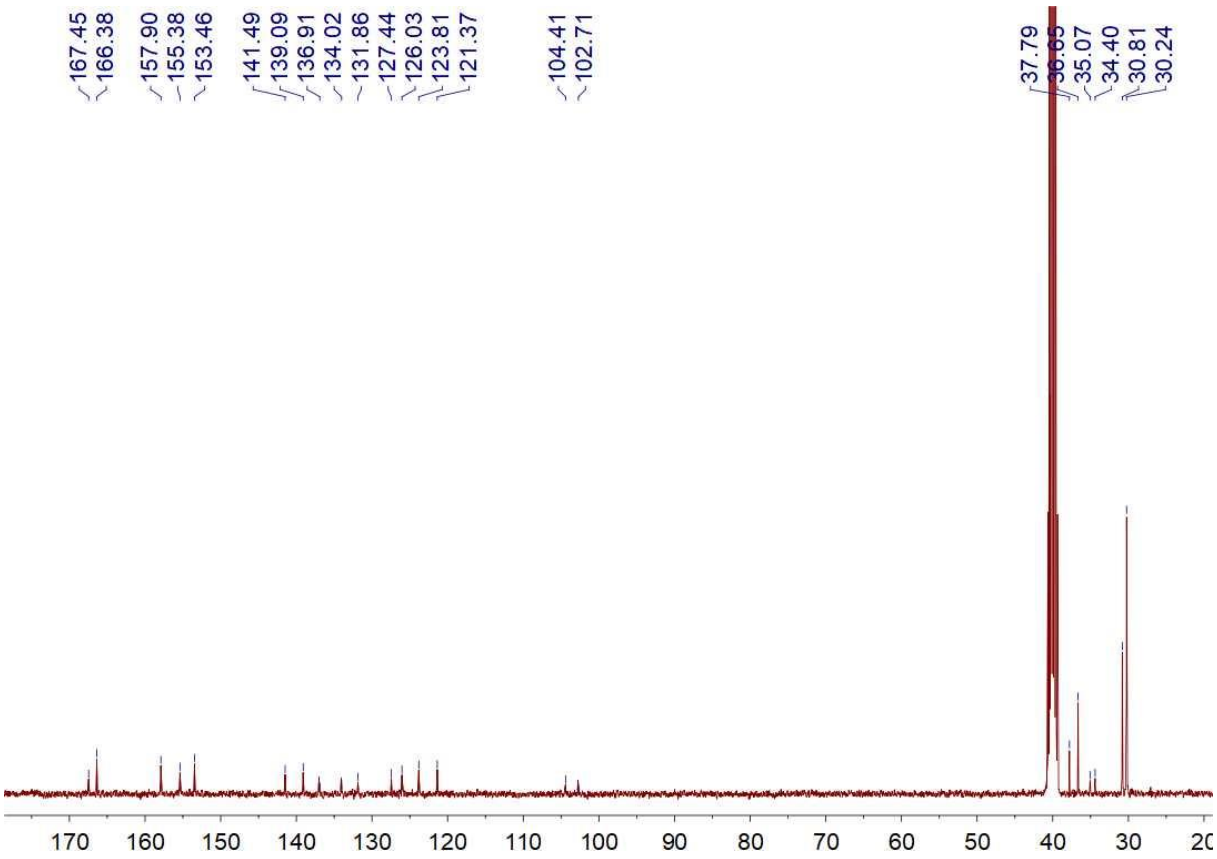

Figure S19. ^{13}C NMR spectrum (100 MHz, d_6-DMSO, 298K) of compound **1**.

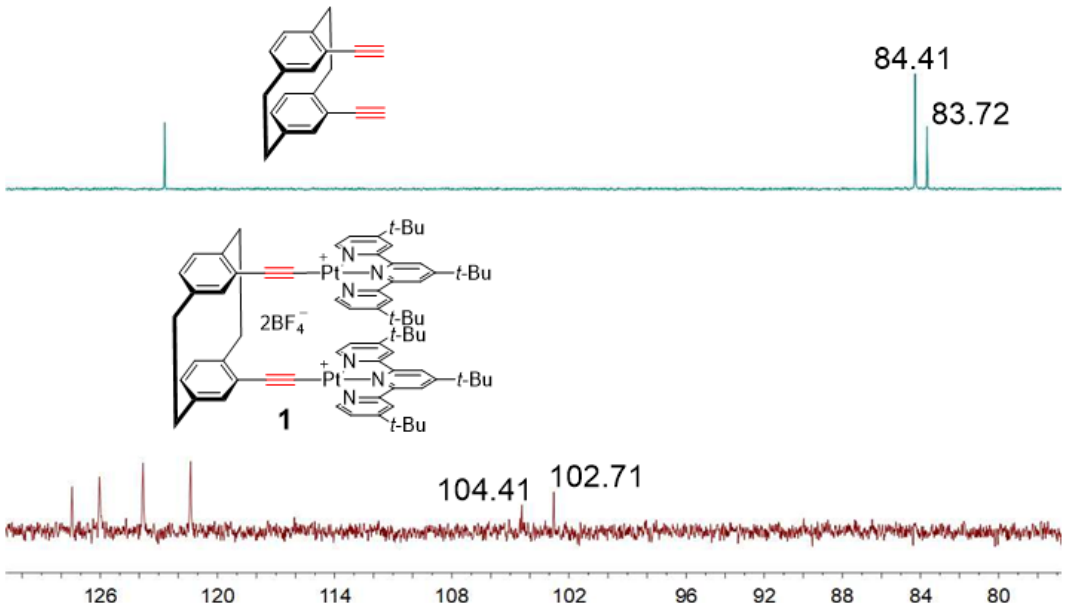

Figure S20. Comparison of ^{13}C NMR spectra (100 MHz, d_6-DMSO, 298K) between compound **1** and 1,5-diethynyl-[2.2]paracyclophane.

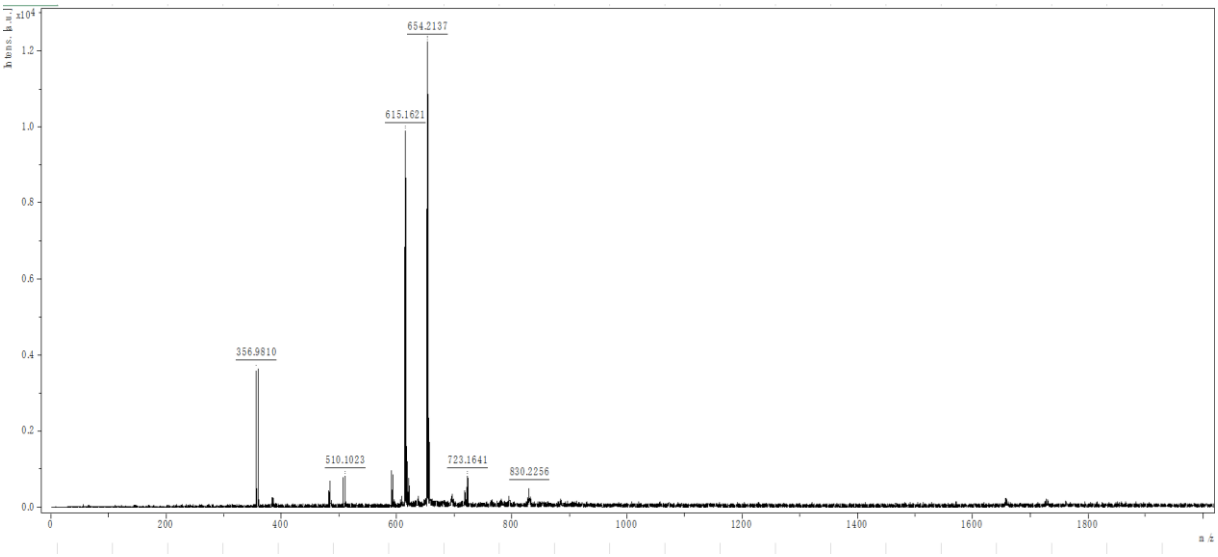

Figure S21. MALDI−TOF−MS spectrum of **1**.

*5.2 Synthesis of compound **2***:

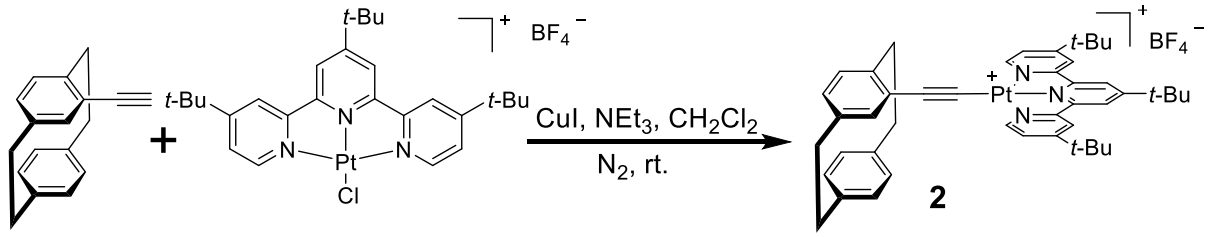

4-Ethynyl[2.2]paracyclophane (50.0 mg, 0.22 mmol), [Pt($N^{t\text{-}Bu}$^$N^{t\text{-}Bu}$^$N^{t\text{-}Bu}$)Cl](BF_4) (0.14 g, 0.20 mmol), CuI (6.0 mg, 0.03 mmol), and NEt_3 (1 mL) in CH_2Cl_2 (10 mL) were stirred at room temperature for 24 hours. The mixture was evaporated under reduced pressure, and the residue was purified by flash column chromatography (Al_2O_3, CH_3OH/CH_2Cl_2, 1 : 100 *v*/*v* as the eluent) to afford **2** as a orange solid (0.15 g, 82%). ^{1}H NMR (400 MHz, $CDCl_3$, 298 K, Figure S22) δ (ppm): 9.25 (d, J = 6.0 Hz, 2H), 8.45 (s, 2H), 8.40 (d, J = 1.7 Hz, 2H), 7.64 (dd, J = 6.0, 1.9 Hz, 2H), 7.20 – 7.17 (m, 1H), 6.62 – 6.51 (m, 4H), 6.47 (s, 2H), 3.81 (ddd, J = 12.9, 10.5, 2.6 Hz, 1H), 3.33 (ddd, J = 12.9, 10.4, 5.2 Hz, 1H), 3.18 – 3.04 (m, 4H), 3.03 – 2.86 (m, 2H), 1.59 (s, 9H), 1.51 (s, 18H). ^{13}C NMR (100 MHz, $CDCl_3$, Figure S23) δ: 168.4, 167.5, 158.9, 153.8, 139.5, 137.7, 133.6, 133.4, 132.8, 131.3, 129.5, 125.3, 123.7, 105.0, 100.2, 70.5, , 37.8, 36.7, 35.6, 35.2, 34.8, 34.5, 30.9, 30.4. MALDI−TOF−MS m/z: $[M–BF_4]^+$ calcd for $C_{45}H_{50}N_3Pt$, 727.3652; found, 727.4442 (Figure S24)

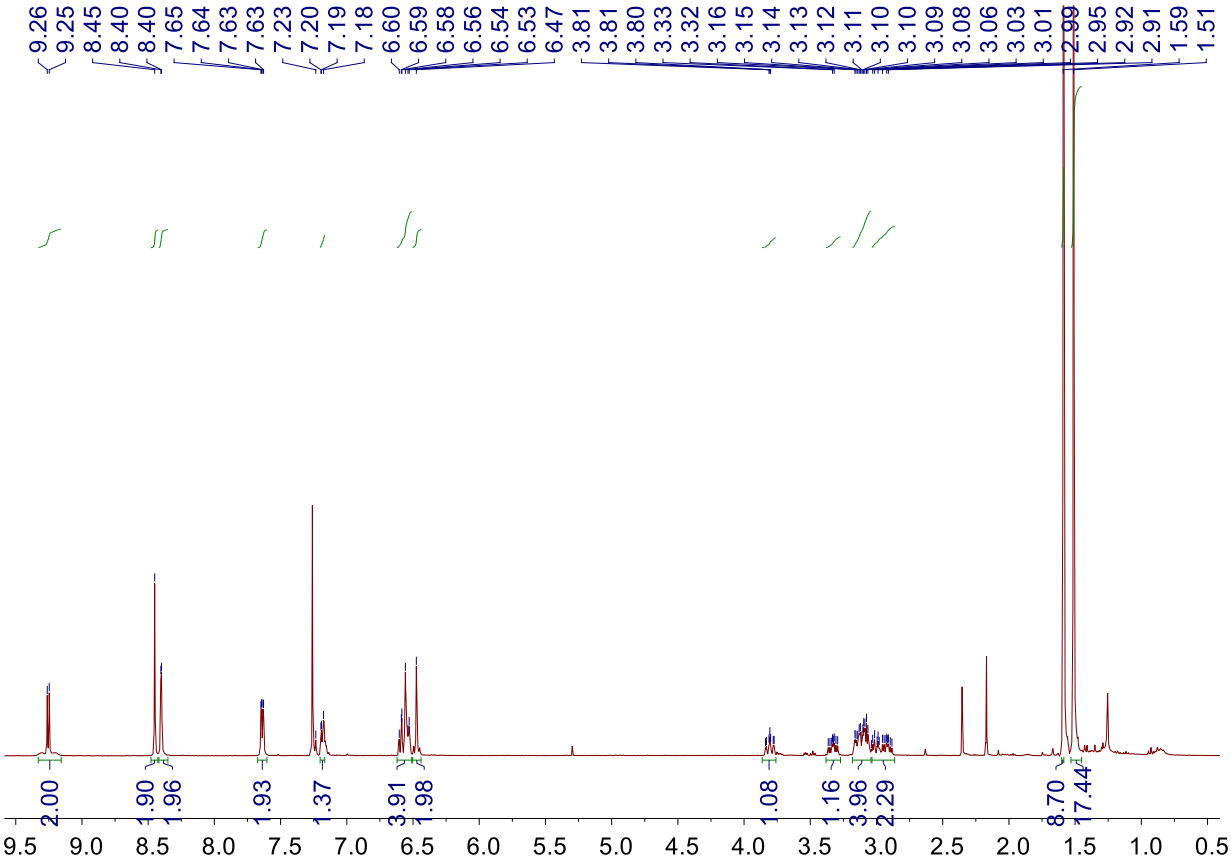

Figure S22. ^{1}H NMR spectrum (400 MHz, $CDCl_3$, 298K) of **2**.

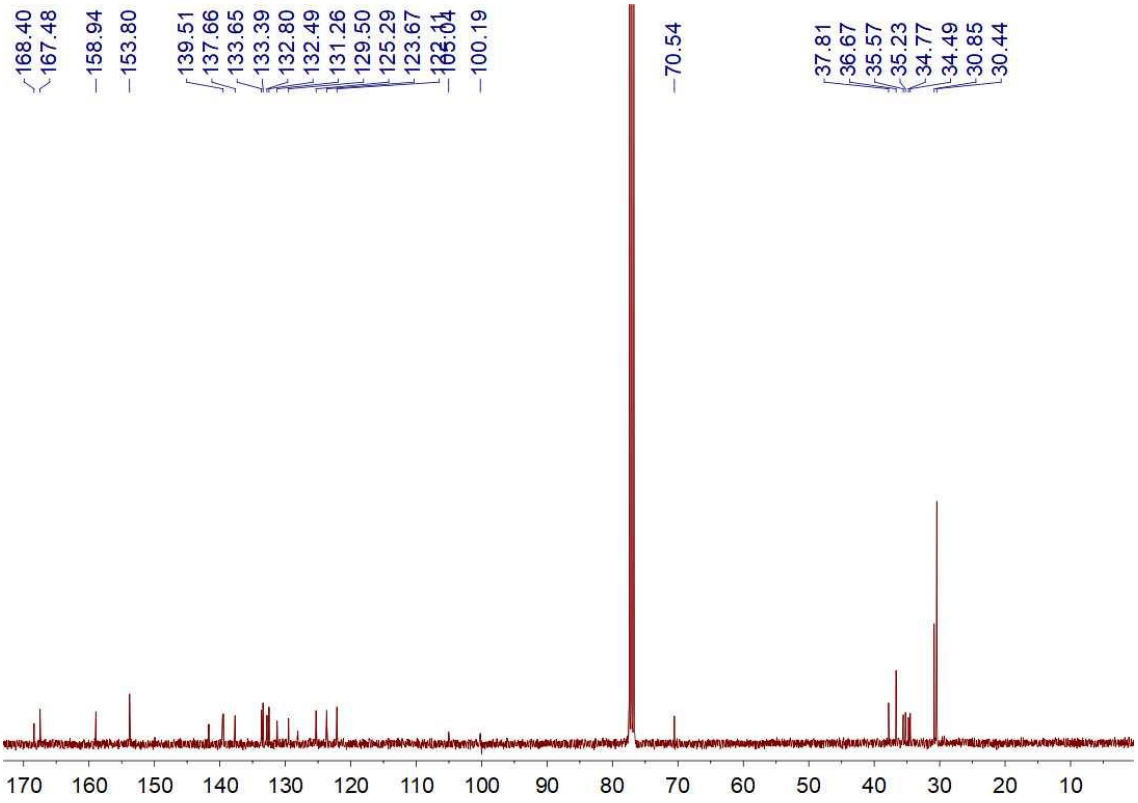

Figure S23. ^{13}C NMR spectrum (100 MHz, $CDCl_3$, 298K) of **2**.

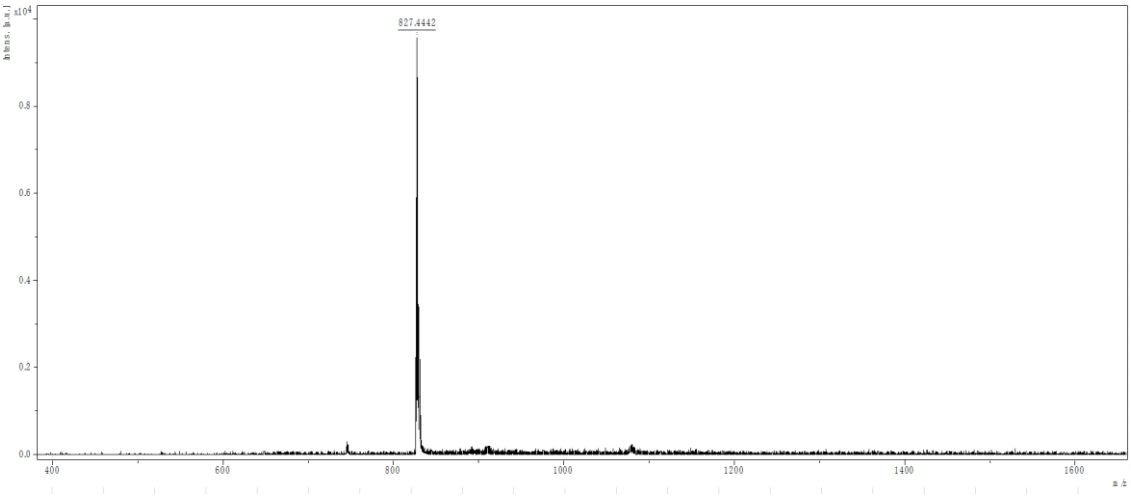

Figure S24. MALDI−TOF−MS spectrum of **2**.

*5.3 Synthesis of compound **4***

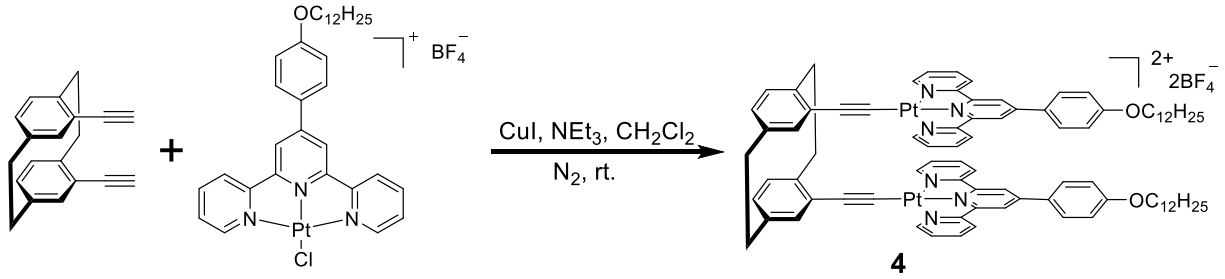

4,15-Diethynyl-[2.2]paracyclophane (50.0 mg, 0.19 mmol), [Pt(N^Nphenyl^N)Cl](BF$_4$) (0.32 g, 0.40 mmol), CuI (10.0 mg, 0.05 mmol), and NEt$_3$ (2 mL) in CH_2Cl_2 (20 mL) were stirred at room temperature for 24 hours. The mixture was evaporated under reduced pressure, and the residue was purified by flash column chromatography (Al_2O_3, CH_3OH/CH_2Cl_2, 1 : 100 *v*/*v* as the eluent) to afford **4** as a dark red solid (0.18 g, 52%). ^{1}H NMR (400 MHz, $CDCl_3$, 298 K, Figure S25) δ (ppm): 9.05 (t, J = 25.0 Hz, 8H), 8.80 (s, 4H), 7.98 (d, J = 8.5 Hz, 4H), 7.78 (d, J = 8.3 Hz, 4H), 7.18 (m, 4H), 6.70 (d, J = 8.6 Hz, 4H), 6.58 (d, J = 4.9 Hz, 4H), 6.43 (d, J = 7.2 Hz, 2H), 3.96 (d, J = 8.1 Hz, 2H), 3.90 (t, J = 7.3 Hz, 4H), 3.15 (d, J = 8.2 Hz, 2H), 3.07 (s, 4H), 1.84 – 1.79 (m, 4H), 1.38 – 1.26 (m, 32H), 0.90 (t, J = 6.6 Hz, 6H). Note that ^{13}C NMR spectrum could not be measured due to the low solubility of **4**. MALDI−TOF−MS *m*/*z*: $[M–2BF_4]^{2+}$ calcd for $C_{86}H_{92}N_6Pt_2O_2$, 815.3289; found, 815.8422 (Figure S26).

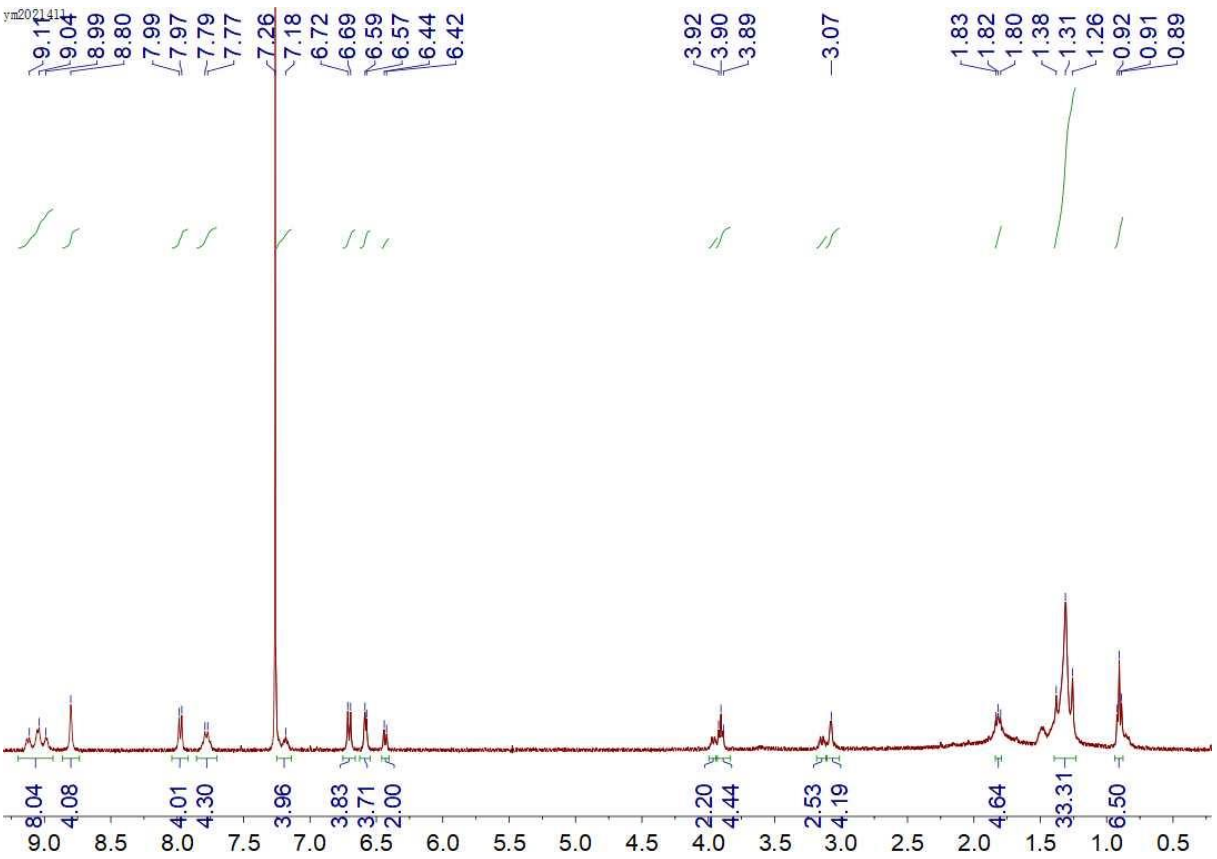

Figure S25. ^{1}H NMR spectrum (400 MHz, $CDCl_3$, 298K) of **4**.

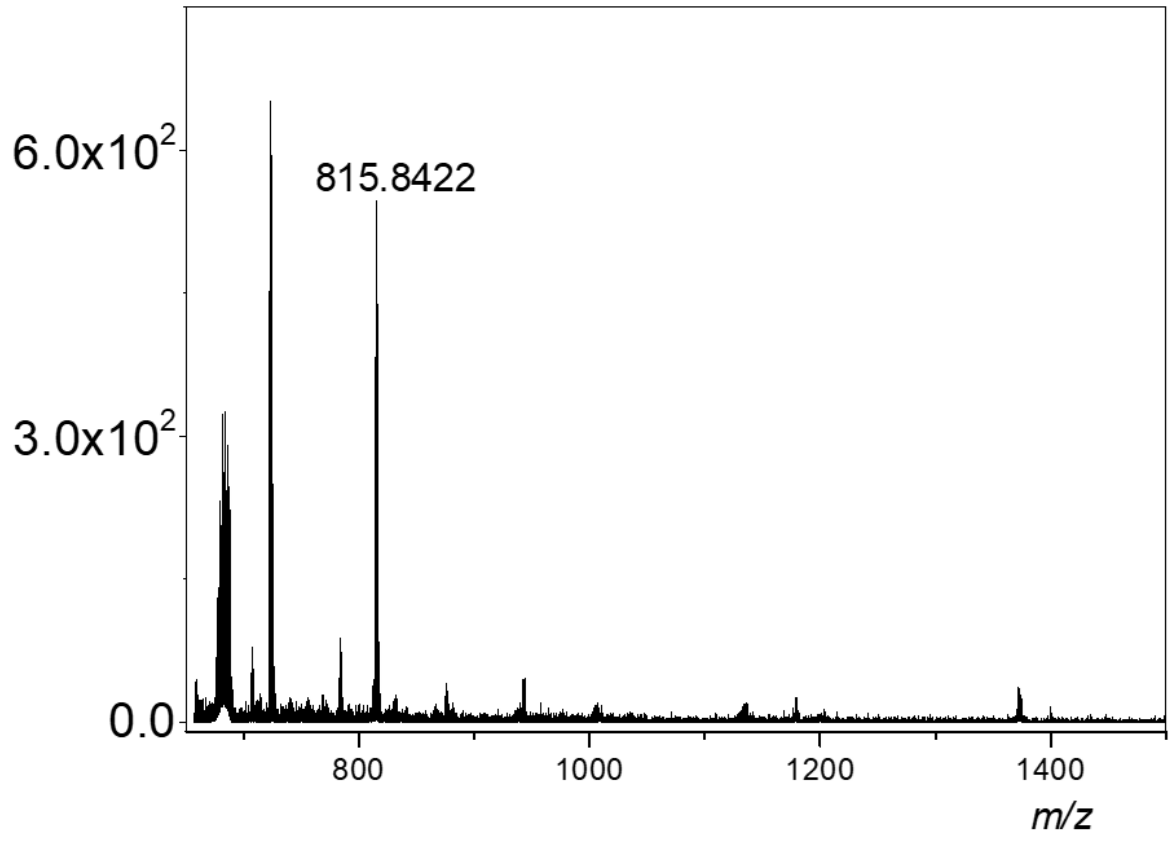

Figure S26. MALDI−TOF−MS spectrum of **4**.

References

[S1] L. Bondarenko, I. Dix, H. Hinrichs, H. Hopf, *Synthesis* 2004, 2751.

[S2] M. Austeri, M. Enders, M. Nieger, S. Brase, *Eur. J. Org. Chem.* 2013, 1667.

[S3] Y.-K. Tian, Y.-G. Shi, Z.-S. Yang, F. Wang, *Angew. Chem. Int. Ed.* 2014, **53**, 6090.

[S4] L-B. Xing, X-J. Wang, X-W. Gao, B. Chen, C-H Tung, L-Z. Wu, *Supramol. Chem.* 2015, **27**, 298.

[S5] P. A. Korevaar, C. Schaefer, T. F. A. de Greef and E.W.Meijer, *J. Am.Chem. Soc*., 2012, **134**, 13482.